Molecular Therapy
Nucleic Acids
Original Article

HMEJ-mediated site-specific integration of a myostatin inhibitor increases skeletal muscle mass in porcine

Mengjing Li,[1,2] Xiaochun Tang,[1,2] Wenni You,[1] Yanbing Wang,[1] Yiwu Chen,[1] Ying Liu,[1] Hongming Yuan,[1] Chuang Gao,[1] Xue Chen,[1] Zhiwei Xiao,[1] Hongsheng Ouyang,[1] and Daxin Pang[1]

[1]Key Laboratory of Zoonosis Research, Ministry of Education, Jilin Provincial Key Laboratory of Animal Embryo Engineering, College of Animal Sciences, Jilin University, 130062 Changchun, Jilin Province, People's Republic of China

As a robust antagonist of myostatin (*MSTN*), follistatin (*FST*) is an important regulator of skeletal muscle development, and the delivery of *FST* to muscle tissue represents a potential therapeutic strategy for muscular dystrophies. The N terminus and FSI domain of *FST* are the functional domains for *MSTN* binding. Here, we aimed to achieve site-specific integration of FSI-I-I, including the signal peptide, N terminus, and three FSI domains, into the last codon of the porcine *MSTN* gene using a homology-mediated end joining (HMEJ)-based strategy mediated by CRISPR-Cas9. Based on somatic cell nuclear transfer (SCNT) technology, we successfully obtained FSI-I-I knockin pigs. H&E staining of longissimus dorsi and gastrocnemius cross-sections showed larger myofiber sizes in FSI-I-I knockin pigs than in controls. Moreover, the Smad and Erk pathways were inhibited, whereas the PI3k/Akt pathway was activated in FSI-I-I knockin pigs. In addition, the levels of *MyoD*, *Myf5*, and *MyoG* transcription were upregulated while that of *MRF4* was downregulated in FSI-I-I knockin pigs. These results indicate that the FSI-I-I gene mediates skeletal muscle hypertrophy through an *MSTN*-related signaling pathway and the expression of myogenic regulatory factors. Overall, FSI-I-I knockin pigs with hypertrophic muscle tissue hold great promise as a therapeutic model for human muscular dystrophies.

INTRODUCTION

Myostatin (*MSTN*) is a member of the transforming growth factor-beta (TGF-β) family that acts as a negative regulator of muscle growth.[1] During development, *MSTN* is expressed at appropriate times and sites to reduce the muscle growth rate without disturbing the establishment of muscle patterning.[2] Mature *MSTN* has been reported to depend on the Smad and mitogen-activated protein kinase (MAPK) signaling pathways to regulate the growth of muscle cells.[3] *MSTN* knockout mice,[4] pigs,[5] and cattle breeds with natural *MSTN* mutations[6] show increased muscle mass, and previous studies have indicated that *MSTN* can be treated as a potential key therapeutic target for GH deficiency-induced skeletal muscle impairment.[7]

As an antagonist of numerous members of the TGF-β family, including *MSTN*, follistatin (*FST*) plays an important role in skeletal myogenesis by promoting the formation and growth of muscle fibers.[8] *FST*, also known as FSH-suppressing protein, is a cysteine-rich, single-chain glycoprotein that was first isolated from bovine and porcine follicular fluid by Robertson and Ueno in 1987.[9] *FST* not only regulates the reproductive activities of animals through the FST/Activin system but also regulates the growth of skeletal muscle through the FST/MSTN system.[10,11] The *FST* gene consists of 6 exons: the first and last exons encode the signal peptide and C terminus, respectively; the second exon encodes the N terminus; and the third, fourth, and fifth exons encode the FSI, FSII, and FSIII domains, respectively. *FST* can generate two major variants through alternative splicing, including a full-length form encoding a 344 amino acid preprotein, and a 317 amino acid protein with a shortened C terminus. After the removal of the signal peptide, a mature protein comprising 315 or 288 amino acids is generated[12] (Figure S1A). The N terminus and FSI domain show the highest affinity for *MSTN*, and the interaction between proteins inhibits the function of *MSTN*, restoring muscle growth.[13,14] Heterozygous *FST* knockout mice show a decline in muscle mass and impairments in muscle regeneration,[15] while transgenic mice with muscle-specific *FST* overexpression exhibit increased skeletal muscle mass.[16] Importantly, when FSI-I-overexpressing mice were crossed with Duchenne muscular dystrophy mice, the resultant DMD/FSI-I mice showed enlarged skeletal muscles.[17] These results suggest that *MSTN* blockade by *FST* is a potential therapeutic strategy for muscular dystrophy.

Received 23 November 2020; accepted 9 June 2021;
https://doi.org/10.1016/j.omtn.2021.06.011.

[2]These authors contributed equally

Correspondence: Hongsheng Ouyang, Key Laboratory of Zoonosis Research, Ministry of Education, Jilin Provincial Key Laboratory of Animal Embryo Engineering, College of Animal Sciences, Jilin University, 130062 Changchun, Jilin Province, People's Republic of China.
E-mail: ouyh@jlu.edu.cn
Correspondence: Daxin Pang, Key Laboratory of Zoonosis Research, Ministry of Education, Jilin Provincial Key Laboratory of Animal Embryo Engineering, College of Animal Sciences, Jilin University, 130062 Changchun, Jilin Province, People's Republic of China.
E-mail: pdx@jlu.edu.cn

Site-specific mutagenesis, substitution, and insertion are considered to have great potential in functional genomics research and gene therapy[18,19] and are typically achieved through CRISPR-Cas9-mediated homologous recombination (HDR).[20,21] The Cas9 protein induces DNA double-strand breaks (DSBs) in the target genome under the guidance of a single guide RNA (sgRNA). In the presence of a repair template that harbors homologous arms (HAs), precise gene editing occurs in which random and multicopy insertion is avoided.[22,23] However, this method is typically inefficient because HDR is only activated in late S/G2 phase.[24] There are many strategies to improve the efficiency of HDR, including blocking the NHEJ pathway by targeting DNA ligase IV with the chemical drug scr7,[25] inhibiting Ku70 and DNA ligase IV expression in the NHEJ repair pathway by RNA interference,[26] overexpressing RAD51 and RAD52, the key factors in the HDR repair pathway,[27] and manipulating the cell cycle.[28] CtIP, a DNA damage response protein, plays a role in the early steps of homologous recombination, and HDR efficiency was shown to increase by fusing the N-terminal domain of CtIP to Cas9.[29] In another, study the use of Cas9 fused to avidin and donors fused to biotin could also achieve higher knockin efficiency due to the affinity between avidin and biotin.[30] However, chemical or genetic interruption of endogenous genes is likely to have potentially harmful effects. A homology-mediated end joining (HMEJ)-based strategy directed by CRISPR-Cas9, which is more efficient than traditional HDR, can achieve precise single base mutations, gene knockouts and gene insertions in the genome. The HMEJ-based strategy requires a repair template containing a gRNA target site on the outer portion of the HA. Subsequently, cleavage by Cas9 at the gRNA target site liberates the donor DNA from the plasmid and exposes 5′ and 3′ homology arms. Yao et al.[31] noted that an HMEJ-based strategy achieved a higher knockin efficiency than conventional HDR, observing a knockin efficiency of *fbrillarin* loci in HEK293T cells and *ACTB* loci in mouse embryos of up to 20%∼30%, approximately 10 times higher than that observed for HDR. Wierson et al.[32] also showed that the integration of exogenous DNA using HMEJ is more efficient than HDR, where the knockin efficiency resulting from HMEJ at *Rosa26* loci (∼23%) in porcine fibroblasts and *AAVS1* loci (∼50%) in K-562 cells was approximately 8∼10 times higher than that of HDR. Compared to the use of chemical drugs, disturbing endogenous genes or fusing elements to Cas9, the HMEJ strategy is safer and easier for obtaining gene knockins. At present, the site-specific knockin approach has been successfully applied in mice,[33,34] rabbits,[35,36] and pigs.[37,38] However, is extremely difficult to produce gene site-specific knockin animals, especially large animals. Knockin mice and rabbits are typically generated through direct zygote injection, which results in chimeric animals with unstable genotypes. Importantly, is costly and time-consuming to obtain stable genotypes through further breeding. Although site-specific knockin pigs produced by somatic cell nuclear transfer (SCNT) avoid technical challenges, such as undesired mosaics, the low HDR efficiency limits its application. Therefore, the HMEJ-based strategy, which exhibits greatly improved knockin efficiency, is likely to be widely used in the generation of genetically engineered pigs.

In the present study, the knockin efficiency mediated by HMEJ and HDR was compared at the pRosa26 and pACTB loci in PFFs. As expected, the HMEJ approach improved the knockin efficiency in porcine fetal fibroblasts (PFFs). Pigs are important as human disease models because of their similar genetic, physiological, and anatomical characteristics to humans.[39,40] To the best of our knowledge, this is the first study to generate site-specific FSI-I-I knockin pigs using the HMEJ strategy. Importantly, FSI-I-I knockin pigs showed increased skeletal muscle mass and hold great promise to serve as therapeutic models of human muscular dystrophies and diabetes.

RESULTS

Comparison of knockin efficiency using traditional HDR and HMEJ methods

The Neon electroporation system, a new generation of electroporation instruments, can efficiently transfect primary cells, stem cells, and cells that are difficult to transfect. For small plasmids, no significant differences were observed in transfection efficiency between the Neon system and older BTX systems. However, the Neon transfection system showed a higher transfection efficiency for larger plasmids (Figures S2 and S3). Therefore, the Neon electroporation system was used in the present study.

To determine whether the HMEJ method could result in improved knockin efficiency compared to HDR in PFFs, we selected the pRosa26 and pACTB loci for validation. First, sgRNAs targeting the pRosa26 and pACTB loci were designed and inserted into CRISPR-Cas9 plasmids (Figures 1A and 1E). To examine the targeting efficiency of the sgRNAs, we electrotransfected the Cas9/sgRNA vectors into PFFs. After 3 days of cultivation, the cells were collected and used as templates for PCR. PCR products encompassing the target site were examined through Sanger sequencing. Multiple obvious peaks were observed surrounding the Cas9 cleavage site in the chromatogram (Figures 1B and 1F), and Tracking of Indels by DEcomposition (TIDE) analysis showed that the total mutation efficiency for the pRosa26 and pACTB loci was 69.3% and 17.8%, respectively (Figures 1D and 1H). To further assess the mutation efficiency, we TA cloned the PCR amplicons and sequenced approximately 100 individual bacterial colonies. The Sanger sequencing results showed mutation efficiencies of 49.5% and 17.8% for the pRosa26 and pACTB loci, respectively, and indels, including insertions, deletions, transitions, and transversions, were observed at the cleavage site (Figures 1C and 1G; Figures S4 and S5). The results indicated that all the sgRNAs efficiently targeted the appropriate sites.

Subsequently, we aimed to insert an SA-EGFP reporter gene into the first intron of the pRosa26 gene and a P2A-EGFP reporter gene into the last codon of the pACTB gene to evaluate knockin efficiency. Both the HDR and HMEJ donors had 800-bp HAs, but the HMEJ donor included sgRNA target sites (Figures 2A and 2D). The percentage of EGFP-positive cells was determined as an indicator of site-specific knockin efficiency. The fluorescence-activated cell sorting (FACS) results showed that the knockin efficiency resulting from HMEJ at pRosa26 and pACTB (20.83% ± 0.7881% and 15.40% ± 0.3606%)

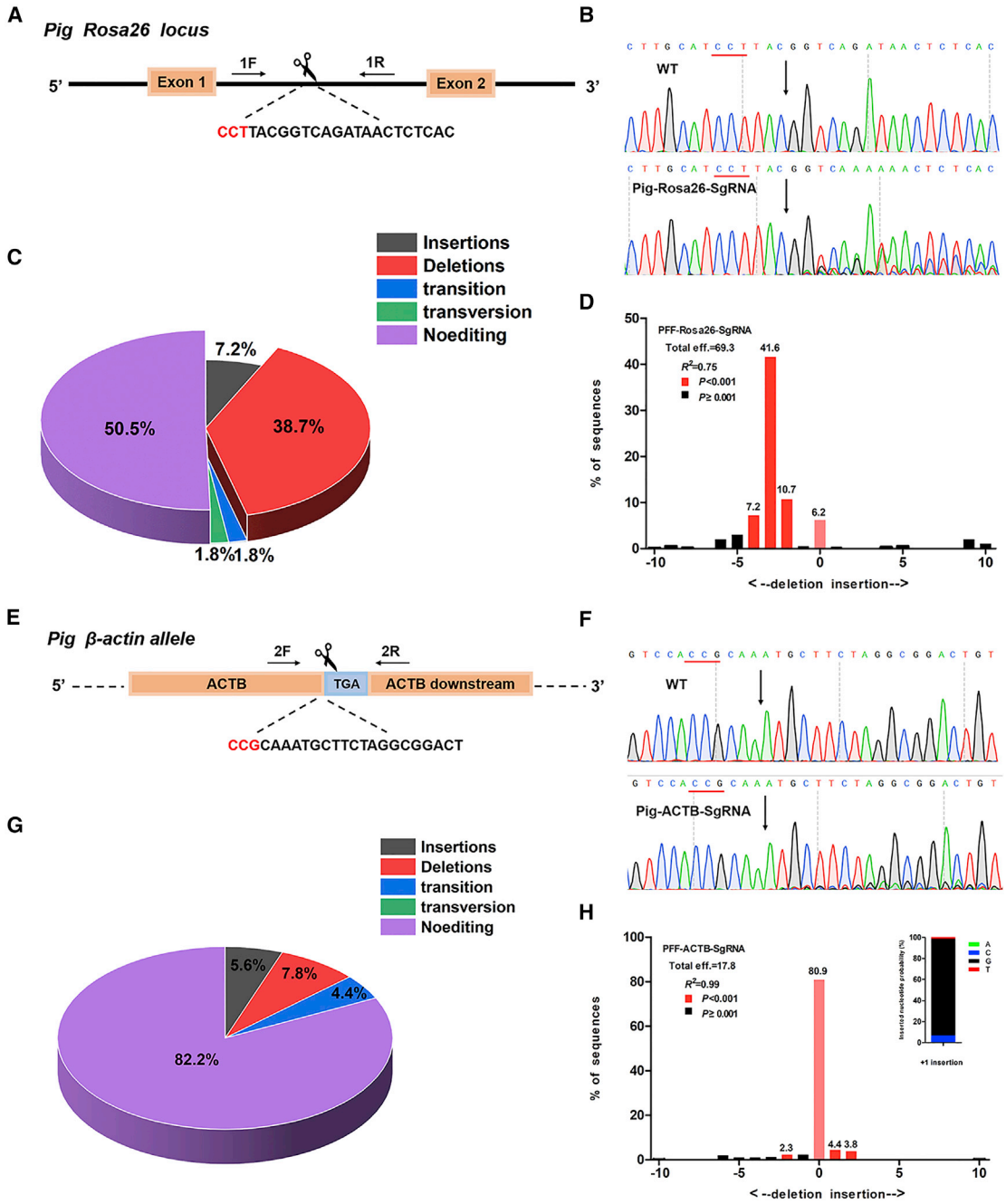

Figure 1. sgRNA design and efficiency evaluation

(A and E) Schematic map of sgRNAs specific to the pRosa26 and pACTB loci. The sgRNA sequence is highlighted in black, and PAM is highlighted in red. (B and F) Sequence chromatogram of CRISPR target regions in electrotransfected cells and wild-type cells. The black arrow indicates the cleavage site, and the PAM is underlined in red. (D and H) A pool of PFFs treated with Cas9 and an sgRNA were analyzed by TIDE. Insets: prediction of the inserted base for +1 insertions. (C and G) The sgRNA-induced indel frequency was examined based on the Sanger sequencing results of approximately 100 TA fragments from an amplicon covering the target sites.

was approximately three times higher than that resulting from HDR (7.69% ± 0.3331% and 4.98% ± 0.2961%) in PFFs (Figures 2B, 2C, 2E, and 2F). Subsequently, EGFP-positive cells from the HMEJ and HDR groups sorted by flow cytometry were expanded in culture, and the EGFP knockin events were further confirmed by PCR with 5′ junction-specific primers. The PCR and Sanger sequencing results confirmed the site-specific integration of EGFP at the pRosa26 and pACTB loci (Figures S6 and S7). Taken together, these results indicate

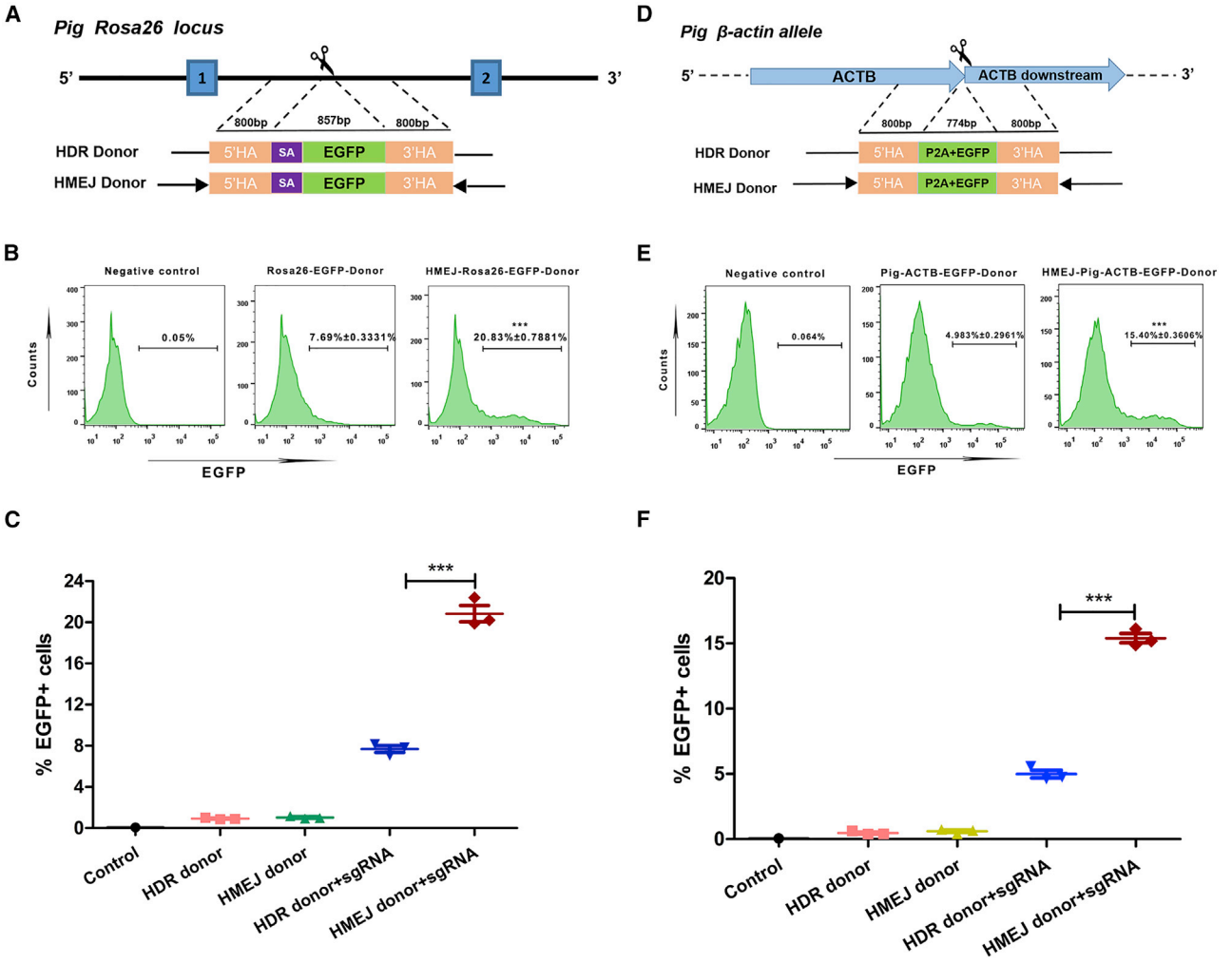

Figure 2. Targeted integration strategy via the HMEJ and HDR methods

(A and D) Schematic overview of the EGFP knockin strategy at different loci. Triangles represent sgRNA target sites, and the SA and P2A sequences are presented in Table S2. (B and E) Percentage of EGFP-positive cells evaluated by FACS. Electroporated cells without vector were used as a negative control; a stable gate was drawn to measure EGFP-expressing cells formed by targeted integration. (C and F) Quantification of EGFP-expressing cells as measured by FACS at day 3. The data from three independent replicates were analyzed with a two-tailed unpaired t test, $^{***}p < 0.001$.

that the HMEJ strategy achieves a higher knockin efficiency than HDR in PFFs.

HMEJ-mediated FSI-I-I site-specific insertion in PFFs

FST consists of a signal peptide, N terminus, FSI domain, FSII domain, FSIII domain, and C terminus (Figure 3A). The phylogenetic tree showed that the *FST* protein is highly conserved among different species. The homology of porcine *FST* with human, mouse, and nonhuman primate *FST* was 97.4%, 96.2%, and 97.7%, respectively (Figure S1B). Importantly, only when the complete N terminus and FSI domain are both present in *FST* can *MSTN* binding occur. A previous study revealed that the overexpression of FST-I-I with an intact N terminus and double FSI domain increased skeletal muscle mass in mice, whereas the overexpression of *FST* with an N-terminal deletion had no effect on muscle quality.[13] Based on this finding, we subsequently aimed to insert FSI-I-I containing the signal peptide, the complete N terminus and the three FSI domains (Figure 3B) in the last codon of the pig *MSTN* (pMSTN) gene (Figure 3C).

An sgRNA targeting the pMSTN locus was designed, and pMSTN-sgRNA/Cas9 cutting activity was assessed, with Sanger sequencing and TIDE analysis results showing an approximately 20.8% mutation efficiency (Figures 3D and 3F). Due to the 31-bp distance between the cutting and the targeting sites, two bases in the seed sequence of the sgRNA sequence in the donor vector were synonymously mutated to prevent the donor vector from being cleaved (Figure 3E). The pMSTN-sgRNA/Cas9 and HMEJ donor plasmids were coelectrotransfected into large white PFFs to screen colonies derived from

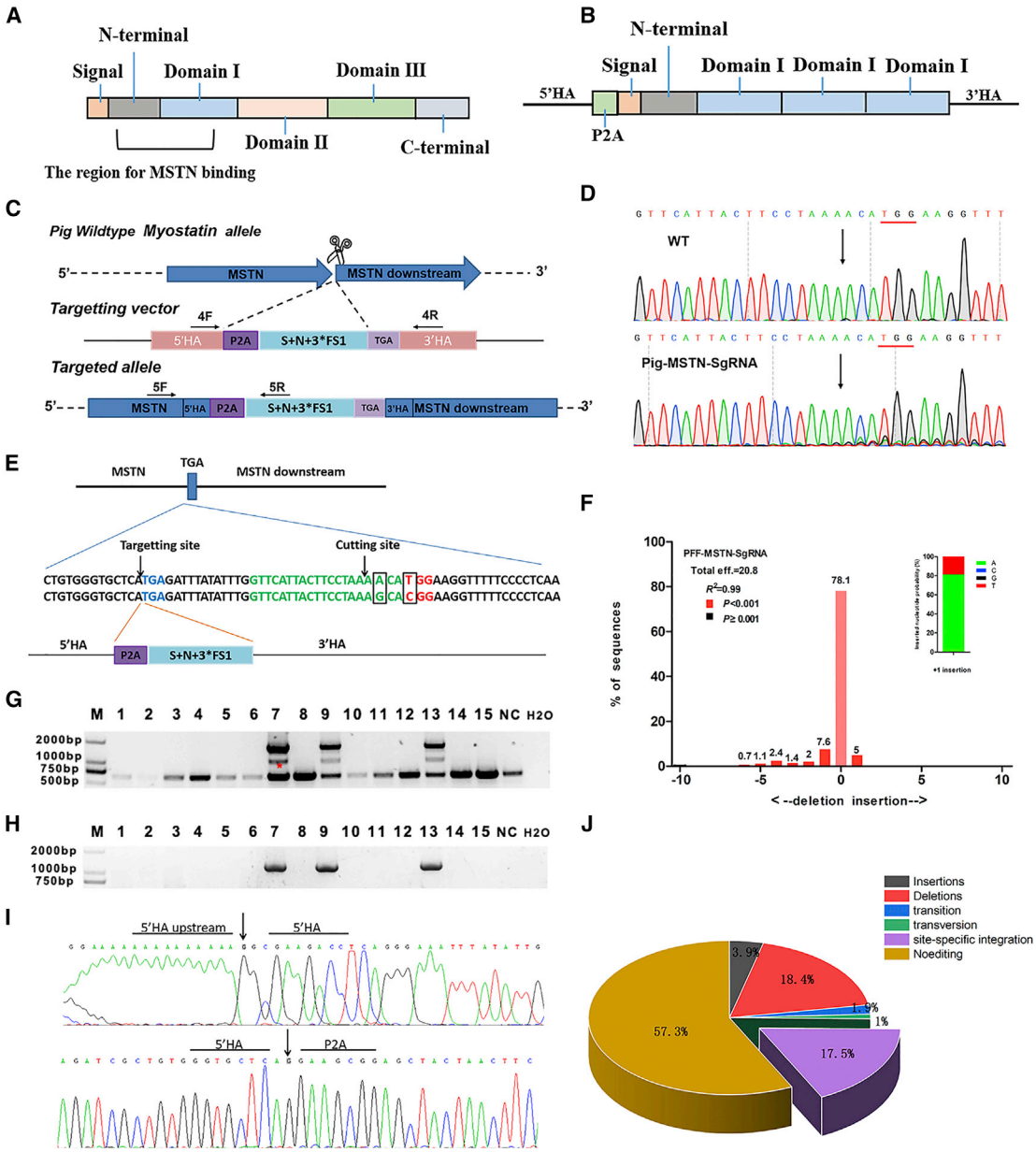

Figure 3. Selection of FSI-I-I knockin colonies derived from single cells

(A) The primary structure of FST protein. (B) The FSI-I-I donor targeted *MSTN* locus. (C) Strategy for FSI-I-I-targeted integration into the *MSTN* locus. (D) Sequence chromatogram of CRISPR target regions in electrotransfected and wild-type PFFs. (E) Schematic diagram of donor vector mutation. The PAM is indicated in red, the sgRNA sequence is indicated in green, and the termination codon is indicated in blue. The mutant base is framed by a rectangle. The first line shows the wild-type sequence, and the next line shows the mutant sequence. (F) TIDE analysis of the pMSTN-sgRNA/Cas9 mutation efficiency. Insertions: prediction of the inserted base for +1 insertions. (G and H) PCR analysis of individual cell clones to identify knockin events. The 4F/R primer was used to identify the insertion of the FSI-I-I gene. If the FSI-I-I gene was integrated into the genome, the PCR amplification fragment was 1,649 bp; otherwise, it was 642 bp. The 5F/R primer pair amplified the 5′ junction. If the FSI-I-I gene integrated the *MSTN* locus in a site-specific manner, the PCR amplification fragment was 1,164 bp; otherwise, there was no band. M, D2000; Lanes 1–15 represent the individual cell clones. NC, wild-type cell clones; H_2O, blank control. The sequences of the primers are listed in Table S1. "*" indicates a hybrid band formed in the process of genomic PCR in heterozygous animals. (I) Sanger sequencing of PCR products using the primers 5F/R. (J) Site-specific integration and NHEJ ratios of 103 individual cell clones. All 103 individual cell clones were analyzed by PCR and sequencing, and genotype statistical analysis was performed.

Table 1. SCNT for the generation of FSI-I-I knockin pigs

Donor cells	Transferred embryos	Pregnancy	Number of births	Number of positive piglets
C4, C5, C6	103	Yes	1	1
C7, C8, C9	101	No	0	0
C7, C8, C9	103	No	0	0
C10, C11, C12	105	Yes	3	2

single cells as previously described.[41] The site-specific integration of FSI-I-I was confirmed by PCR with primers targeting regions inside and across HAs (Figure 3A). The agarose gel electrophoresis and sequencing results for the PCR products indicated that all the positive clones were heterozygous (Figures 3G–3I). To further confirm HMEJ efficiency, we genotyped 103 selected colonies derived from single cells and observed site-specific integration in 17.8% of them (Figure 3J). The sequencing results for colonies derived from single cells with indels are shown in Figure S8. The results showed that indels, including insertions, deletions, transitions, and transversions, were present in the pMSTN cleavage site.

Generation and genotyping of gene-modified pigs

FSI-I-I knockin large white PFFs were used as donor cells for SCNT, and approximately 400 reconstructed embryos were transferred to four surrogates (Table 1), with the SCNT workflow shown in Figure 4A. Prior to SCNT, we tested the blastocyst development rate to ensure that the positive clones would not affect embryo development. As expected, the positive reconstructed embryos exhibited a blastocyst development rate similar to that of the wild-type reconstructed embryos (19.27% ± 0.9135% versus 20.20% ± 0.8145%, $p > 0.05$, $n = 3$) (Figure 4B; Table 2). Approximately 114 days after embryo transfer, the two pregnant sows gave birth to 4 cloned piglets, three of which were identified as FSI-I-I knockin positive by PCR and Sanger sequencing (Figures 4C–4E). To determine whether the FSI-I-I gene was randomly integrated into the porcine genome, the 5′HA copy number in FSI-I-I knockin and wild-type pigs was determined. If random integration occurs, 5′HA, FSI-I-I and 3′HA will all be integrated into the porcine genome. As expected, the qPCR results confirmed that there was no random integration of the FSI-I-I gene in cloned pigs (Figure 4F). Off-target effects have always been an important issue hindering the widespread application of gene editing. Therefore, 8 potential off-target sites (OTSs) were selected, and specific primers were designed to amplify the corresponding regions. T7E1 analysis and sequencing results revealed no off-target effects (Figure S9).

FSI-I-I expression increases skeletal muscle mass in genetically modified pigs

Eleven F1 generations were obtained from the cross-breeding of the FSI-I-I knockin pigs and large white boars, five of which included positive heterozygous offspring (Figures 5A and 5B), indicating that the transgene can be stably transmitted to offspring. In addition, 3-month-old knockin pigs with FSI-I-I expressed in muscle exhibited wider backs, larger buttock muscles, and visible grooves under the skin in the limbs (Figure 5C). To investigate the effect of the *MSTN* downstream pathway on muscle growth, we slaughtered three FSI-I-I knockin pigs and three wild-type controls at 3 months of age and performed real-time PCR to quantify FSI-I-I and *MSTN* expression at the transcriptional level. FSI-I-I was integrated into the last codon of *MSTN*, and the two fragments were separated by P2A. The levels of FSI-I-I and *MSTN* transcription were consistent in different tissues, with the highest levels observed in the longissimus dorsalis (Figure 5D). In addition, no significant difference in *MSTN* expression was detected among different skeletal muscle tissues, including the longissimus dorsi, gastrocnemius muscle, trapezius pectoralis, triceps brachii, biceps femoris, and semitendinosus, which are primarily located in the back, limbs, and buttocks (Figures 5E and 5F). These results indicated that FSI-I-I expression was consistent in different skeletal muscle tissues. Therefore, the longissimus dorsi and gastrocnemius muscles were selected for subsequent analysis. H&E staining of longissimus dorsi and gastrocnemius muscles cross-sections showed that myofiber size in FSI-I-I knockin pigs was larger than that in the controls (Figures 5H and 5J). Approximately 200 myofibers from each pig were randomly selected for measurement, and myofiber area distribution frequency diagrams were generated. The number of longissimus dorsi myofibers distributed in a 300–600 μm^2 area in wild-type pigs was higher than that observed in knockin pigs, whereas the number of longissimus dorsi myofibers distributed in a >800 μm^2 area of wild-type pigs was lower than that observed in knockin pigs (Figure 5G). The number of gastrocnemius myofibers distributed in a 300–1,100 μm^2 area in wild-type pigs was higher than that observed in knockin pigs, while the number of gastrocnemius myofibers distributed in a >1,300 μm^2 area in wild-type pigs was lower than that observed in knockin pigs (Figure 5I).

Subsequently, proteins were extracted from the longissimus dorsalis muscles of knockin and wild-type pigs, and the level of *MSTN* expression was not observed to change due to FSI-I-I integration (Figures 6A and 6B). The expression of endogenous *FST* protein, but not FSI-I-I, remained consistent (Figures 6C and 6D). Mature *MSTN* has been reported to bind serine/threonine kinase type II receptors (ActRIIB) to activate downstream signal transduction, resulting in Smad2 and Smad3 phosphorylation.[42] Yang et al.[43] showed that *MSTN* negatively regulates myogenic differentiation by activating the Erk1/2 cascade, which results in Erk1/2 phosphorylation, with other reports having shown that of *MSTN* inhibition increases AKT phosphorylation.[44] In our present study, the ratios of phosphorylated Smad2 (p-Smad2) to total Smad2 and of p-Smad3 to total Smad3 were lower in FSI-I-I knockin pigs than in wild-type pigs ($p < 0.05$; Figures 6E–6H). Moreover, the ratio of p-Erk1/2 to total Erk1/2 was significantly lower in FSI-I-I knockin pigs than in wild-type pigs ($p < 0.0001$; Figures 6I and 6J). In contrast, the ratio of p-AKT to total AKT was higher in FSI-I-I knockin pigs than in wild-type pigs ($p < 0.0001$; Figures 6K and 6L). The observed inhibition of the Smad and ERK pathways and activation of the AKT pathway indicated that *MSTN* activity was inhibited in FSI-I-I knockin pigs.

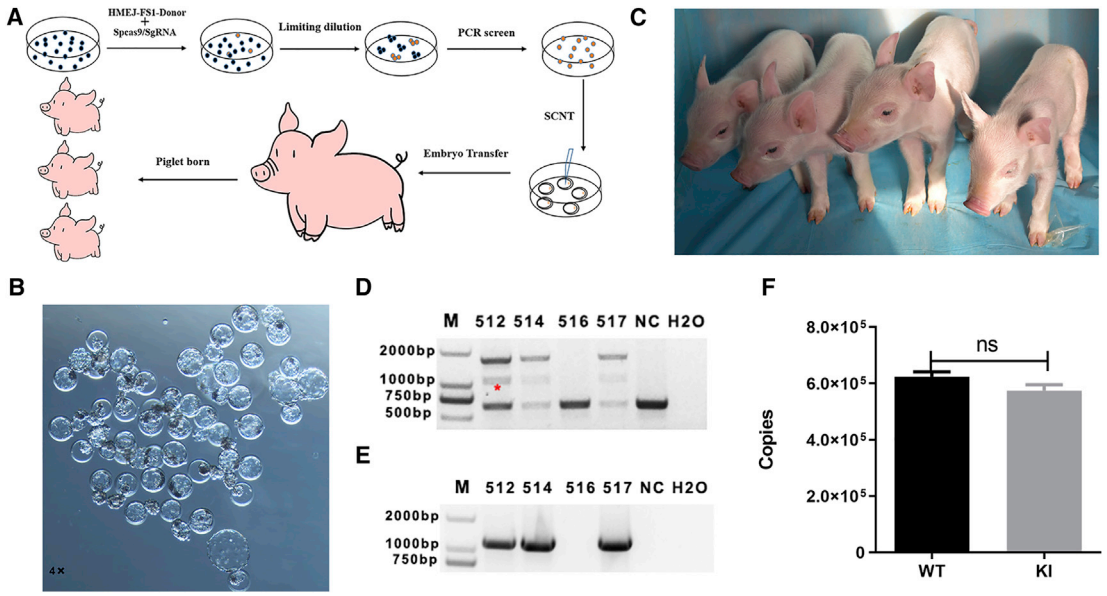

Figure 4. Generation of FSI-I-I knockin pigs through SCNT

(A) Flow chart of the experimental procedures for preparing FSI-I-I knockin pigs. (B) Statistical analysis of the blastocyst development rate of positive and wild-type clones after 6 days of nuclear transfer. (C) Image of 4-day-old piglets. (D and E) PCR results for cloned pigs using the primer pairs 4F/R and 5F/R. The primers 4F/R were used to identify the insertion of the FSI-I-I gene. If the FSI-I-I gene was integrated into the genome, the PCR amplification fragment was 1,649 bp; otherwise, it was 642 bp. The 5F/R primer pair amplified the 5′ junction. If the FSI-I-I gene integrated the *MSTN* locus in a site-specific manner, the PCR amplification fragment was 1,164 bp; otherwise, there was no band. M, D2000; Lanes 1–4 represent the cloned pigs. NC, wild-type pigs; H_2O, blank control. "*" indicates a hybrid band formed in the process of genomic PCR in heterozygous animals. (F) Copy number detection of the *MSTN* gene. The copy number of the *MSTN* gene was detected using the standard curve method, and the *MSTN* amplicons were specific for 5′HA.

Myogenic regulatory factors (MRFs) play key roles in skeletal muscle commitment and differentiation and comprise four members: *MyoD*, *Myf5*, *MyoG*, and *MRF4*. *MyoD* and *Myf5* have a crucial role in the development of myogenic cells; *MyoG* is involved in the differentiation of progenitors into myofibers; and *MRF4* is involved in myofiber maturation.[45] In our present study, the levels of *MyoD* ($p < 0.0001$), *Myf5* ($p < 0.001$), and *MyoG* ($p < 0.0001$) transcription were higher, whereas that of *MRF4* ($p < 0.0001$) was lower in FSI-I-I knockin pigs than in wild-type pigs. In addition, the levels of *MyoD* and *Myf5* transcription were extremely low, while that of *MRF4* was the highest in 3-month-old pigs (Figure 6M).

DISCUSSION

The site-specific integration of target genes has been widely used to generate genetically modified pigs to assess target gene function and establish animal models.[37,38,46] Furthermore, the site-specific integration strategy does not introduce selection marker genes, decreasing public concern regarding the biosafety of genetically modified animals and increasing their agricultural application. However, the site-specific knockin of target genes mediated by HDR is typically inefficient. Importantly, although previous reports have shown that NHEJ and DNA-PKcs inhibitors can increase the HDR frequency,[47,48] Xie et al.[49] they cannot improve HDR efficiency in PFFs. HMEJ shows a higher gene knockin efficiency than HDR in HEK293T cells, hepatocytes, primary astrocytes, neurons, K-562 cells, and porcine fibroblasts.[31,32] In the present study, the knockin efficiency resulting from HMEJ and HDR was compared at the pRosa26 and pACTB loci in PFFs. As expected, the site-specific integration rate mediated by HMEJ was approximately three times higher than that resulting from HDR at the pRosa26 and pACTB loci in PFFs. At present, fetal fibroblasts have been used as the first choice of donor cells for SCNT because of their ability to be manipulated through electrofusion or lipid transfection.[50] Lee et al.[51] showed that the blastocyst rate obtained using porcine fetal fibroblasts as nuclear donors was significantly higher than that of other cells, such as adult fibroblasts, cumulus cells, and oviduct epithelial cells. Therefore, the increased efficiency of site-specific integration of foreign genes in PFFs is of great significance with respect to conserving resources and labor for the generation of precise gene knockin pigs. Generally, the HMEJ-based strategy is robust for targeted gene integration in PFFs and holds great promise for the generation of large animals with precise gene knockins.

The inhibition of *MSTN* activity promotes increase muscle mass and prevents muscle degeneration, indicating that targeting *MSTN* would be an appropriate therapeutic method for degenerative muscle diseases such as muscular dystrophy and cachexia.[52,53] *FST* has been widely used as an antagonist of *MSTN* to increase skeletal muscle mass in model animals and has great potential for use in the treatment of muscular atrophy. Muscle overexpression of *FST*

Table 2. *In vitro* development of reconstructed embryos

Donor cells	Number of oocytes used for SCNT	Number of reconstructed embryos	Number developed to blastocysts	Blastocyst rate
FS1-C1	300	290	52	17.9%
FS1-C2	310	290	55	18.9%
FS1-C3	310	290	61	21%
WT-C1	320	290	63	21.7%
WT-C2	310	290	58	20%
WT-C3	310	290	55	18.9%

via adeno-associated virus (AAV) delivery was observed to induce hypertrophy compared to the control.[54] In another study, FSI-I transgenic *mdx* mice with a muscle-specific promoter were shown to exhibit increased skeletal muscle mass and ameliorated dystrophic pathology.[13,16,17] In addition, *FST* transgenic pigs with a skeletal muscle-specific promoter show enhanced skeletal muscle growth.[55] However, all previously reported *FST* transgenic animals were generated using traditional transgenic methods, which often cause unpredictable gene expression, genetic changes, and unstable phenotypes.[56] The number and the location of exogenous genes inserted into the host genome affects the expression of transgenes. The site-specific integration approach can be used to insert an exogenous gene into a targeted locus with minimal impacts on the genomic structure or protein expression of nearby genes. In addition, endogenous regulators can be used to conditionally express exogenous genes.[57] Therefore, a site-specific integration strategy is essential for the generation of transgenic animals. In our present study, we prepared a transgenic pig using the HMEJ method directed by CRISPR-Cas9, and the F1 generations were born healthy, demonstrating that the transgene could be stably transmitted to offspring. In these transgenic pigs, FSI-I-I was integrated into the last codon of *MSTN,* and the two fragments were separated by P2A, which led to the expression of FSI-I-I driven by the porcine endogenous *MSTN* promoter. Furthermore, FSI-I-I and *MSTN* were expressed at similar levels in developing muscle.

The N terminus and FSI and FSII domains of *FST* primarily contribute to the binding affinity of this protein. The N terminus and FSI domain of *FST* are the functional domains for *MSTN* binding, whereas the FSII domain is critical for high-affinity interaction with activin A. Activin A is involved in many physiological functions, such as reproduction,[58] glucose metabolism,[59–62] the differentiation of nerve cells,[63] and immunity.[64] Thus, blocking activin A may have adverse side effects on the organism. In our present study, we chose the N terminus and FSI domain rather the entire *FST* gene to generate knockin pigs, which avoided altering the normal functions. Moreover, the knockin gene fragment was derived from the *FST* gene of pigs rather than other species, minimizing the adverse effects of gene knockin on pigs. As off-target effects may disturb nontarget genes, they are a primary focus of CRISPR-Cas9-mediated gene editing.[65] Our results showed that no off-target effects were detectable in the cloned pigs, suggesting that pig-MSTN-sgRNA exhibited high specificity.

Piedmontese and Belgian blue cattle carrying a naturally mutated *MSTN* gene, pigs with *MSTN* knockout and pigs overexpressing human *FST* exhibit increased skeletal muscle mass.[5,55,66,] In our present study, transgenic pigs with muscle-specific expression of FSI-I-I in exhibited similar phenotypes, such as hypertrophic muscle tissue (primarily in the hindquarters), intramuscular boundaries and visible grooves under the skin, and wider backs. As the endogenous *MSTN* promoter drives FSI-I-I expression, the levels of FSI-I-I and *MSTN* transcription are consistent in different tissues, with the highest level occurring in the longissimus dorsi. Because of the consistent *MSTN* expression among different skeletal muscle tissues, the function of the FSI-I-I gene in different skeletal muscles is consistent. Using the longissimus dorsi and gastrocnemius as representative muscles, the cross-sectional area of muscle fibers was analyzed, and the results showed that the myofiber size of FSI-I-I knockin pigs was larger than that of control pigs in the same litter. TGF-β superfamily ligands have been reported to mediate signal conduction by binding different cell receptors, thereby affecting the canonical Smad pathway and non-Smad pathways.[67] In the present study, the Smad signaling and Erk pathways were inhibited, while the PI3k/Akt pathway was activated in FSI-I-I knockin pigs, indicating that the function of *MSTN* was inhibited. The myogenic regulatory factors *MyoD* and *Myf5* have crucial roles in the development of myogenic cells, with an absence of desmin-expressing myoblast-like cells having been observed in transgenic mice carrying mutant *MyoD* and *Myf5* genes.[68] *MyoG* is involved in the differentiation of progenitors into myofibers, and *MRF4* is involved in myofiber maturation. *MyoG*-deficient mice show significantly decreased muscle mass,[69] while *MRF4* knockdown in adult rat muscle causes myofiber hypertrophy.[70] In our present study, the levels of *MyoD* and *Myf5* transcription were extremely low, while that of *MRF4* was the highest in FSI-I-I knockin pigs. In addition, *MyoD*, *Myf5*, and *MyoG* transcription was upregulated, whereas that of *MRF4* was downregulated in FSI-I-I knockin pigs. These results indicate that the FSI-I-I gene mediates skeletal muscle hypertrophy by upregulating *MyoD*, *Myf5*, and *MyoG* expression and suppressing that of *MRF4*. Because of the robust antagonism of *MSTN* by FSI-I-I, FSI-I-I knockin pigs can be used to promote livestock breeding with the aim of obtaining a higher percentage of lean meat.

Muscle wasting diseases such as Duchenne muscular dystrophy, cachexia, and sarcopenia are often accompanied by muscle insulin resistance. Previous studies have shown that *FST* overexpression induces skeletal muscle hypertrophy and increases insulin secretion in the muscles of mice with diet-induced obesity.[54] *MSTN* and actin A are upregulated in obesity-related patterns and are involved in muscle atrophy and inflammation.[71] Interestingly, the inhibition or gene deletion of *MSTN* and actin A, which are *FST* targets, protects against high-fat-diet-induced obesity.[72,73] Furthermore, AAV-mediated *FST* delivery to muscle tissue increases muscle formation while alleviating obesity-induced osteoarthritis in mice.[74] Thus, *FST* overexpression

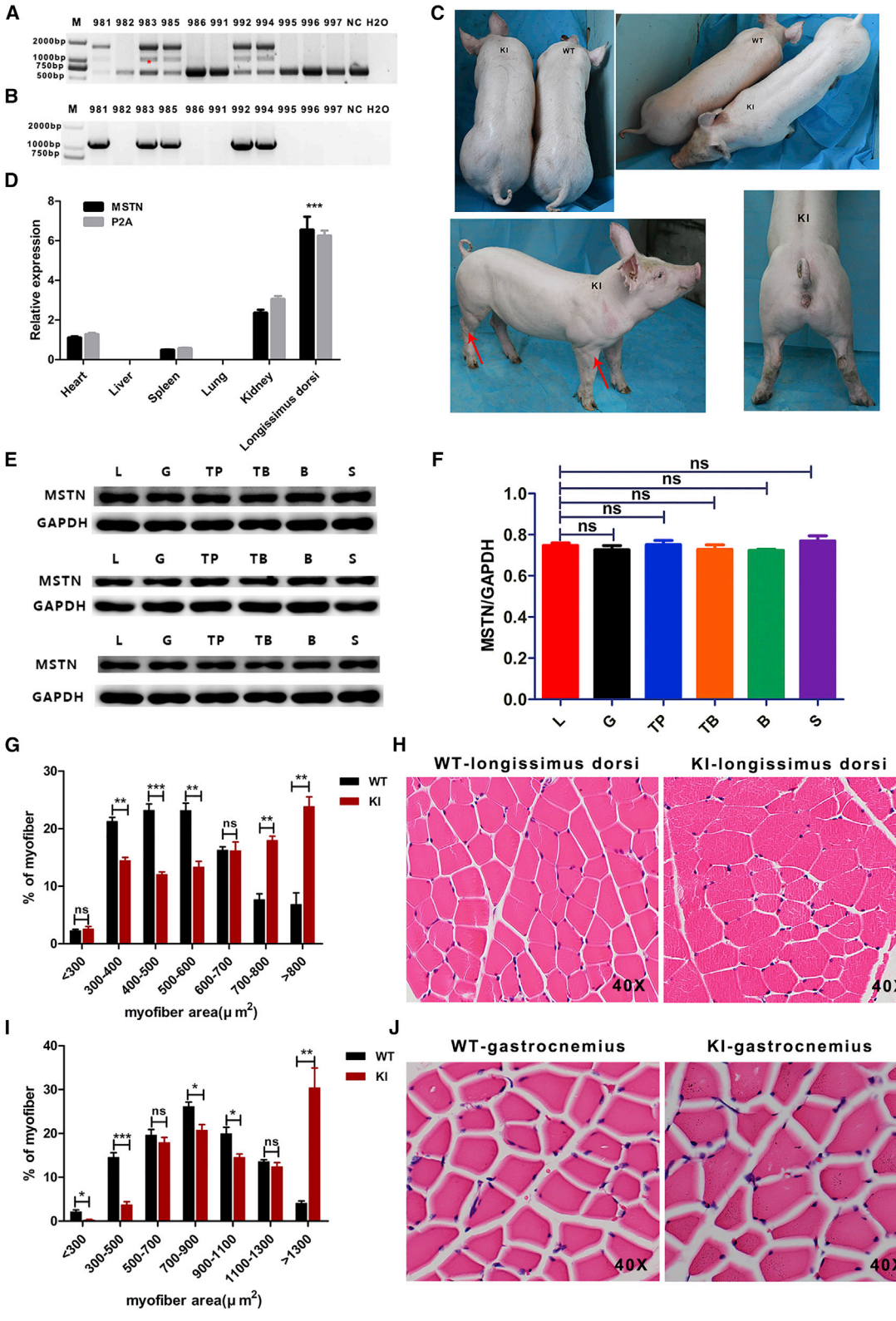

(legend on next page)

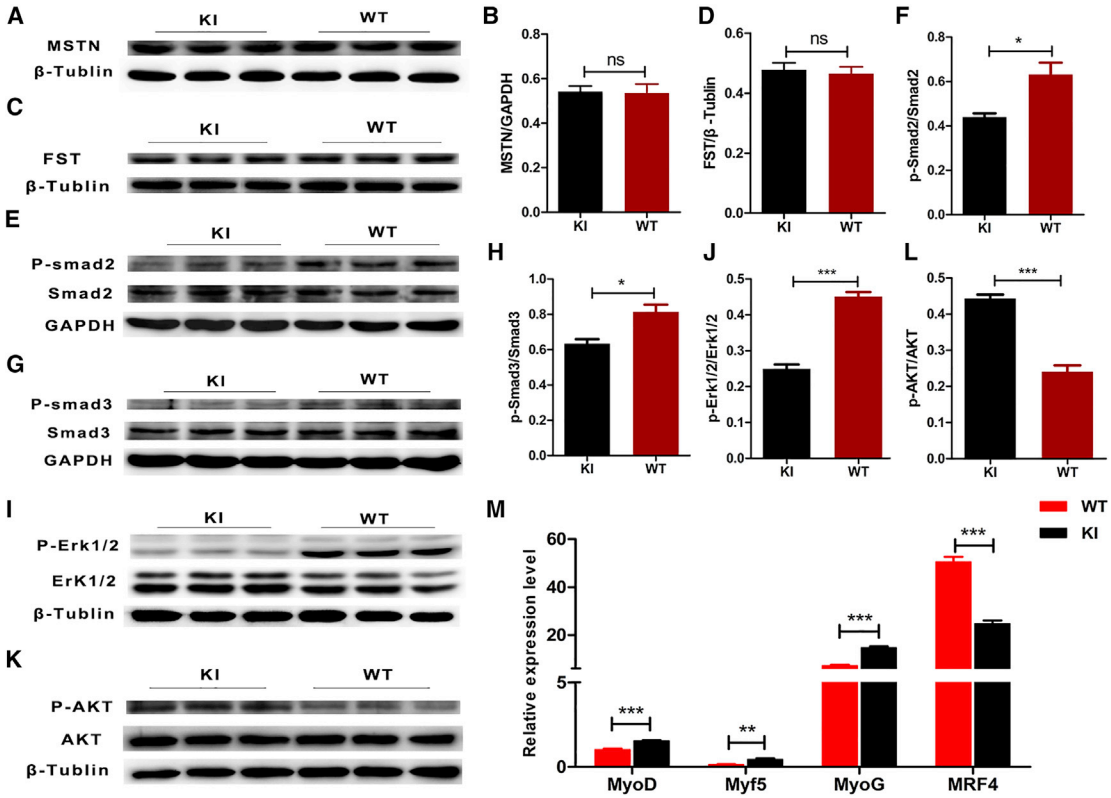

Figure 6. Detection of Smad, Erk, and AKT pathway proteins and myogenic regulatory factors in the longissimus dorsi of FSI-I-I knockin and wild-type pigs

(A and B) Western blot and gray value analysis of *MSTN* expression in the longissimus dorsi of FSI-I-I knockin and wild-type pigs. The gray value analysis of protein bands was performed using ImageJ. A two-tailed unpaired t test was used for statistical analysis, n = 3, $*p < 0.05$, $**p < 0.01$, $***p < 0.001$. (C and D) Western blot and gray value analysis of endogenous *FST* expression in the longissimus dorsi of FSI-I-I knockin and wild-type pigs. (E and F) Western blot and gray value analysis of Smad2 and p-Smad2 proteins in the longissimus dorsi of FSI-I-I knockin and wild-type pigs. Compared to the control group, the expression of p-Smad2 to total Smad2 was significantly decreased in FSI-I-I knockin pigs. (G and H) Western blot and gray value analysis of Smad3 and p-Smad3 proteins in the longissimus dorsi of FSI-I-I knockin and wild-type pigs. Compared to the control group, the expression of p-Smad3 to total Smad3 was significantly decreased in FSI-I-I knockin pigs. (I and J) Western blot and gray value analysis of Erk1/2 and p-Erk1/2 proteins in the longissimus dorsi of FSI-I-I knockin and wild-type pigs. Compared to the control group, the expression of p-Erk1/2 to total Erk1/2 was significantly decreased in FSI-I-I knockin pigs. (K and L) Western blot and gray value analysis of AKT and p-AKT proteins in the longissimus dorsi of FSI-I-I knockin and wild-type pigs. Compared to the control group, the expression of p-AKT to total AKT was significantly upregulated in FSI-I-I knockin pigs. (M) The transcriptional level of myogenic regulatory factors in the longissimus dorsi of FSI-I-I knockin and wild-type pigs. Compared to the control group, the levels of *MyoD*, *Myf5*, and *MyoG* transcription were significantly upregulated, whereas that of MRF4 was downregulated.

can be used as a therapeutic strategy for the treatment of muscle atrophy, insulin resistance in muscle wasting diseases, and metabolic inflammation in obesity. In our present study, FSI-I-I knockin downstream of the *MSTN* gene significantly inhibited *MSTN* function and increased the skeletal muscle mass of pigs. Importantly, pigs are considered good animal models for studying human diseases because

Figure 5. FSI-I-I knockin pigs exhibit increased skeletal muscle mass

(A and B) PCR identification of F1 generation offspring using primer pairs 4F/R and 5F/R. The 4F/R primer pair was used to identify the insertion of the FSI-I-I gene. If the FSI-I-I gene was integrated into the genome, the PCR amplification fragment was 1,649 bp; otherwise, it was 642 bp. The 5F/R primer pair amplified the 5′ junction. If the FSI-I-I gene integrated the *MSTN* locus in a site-specific manner, the PCR amplification fragment was 1,164 bp; otherwise, there was no band. M, D2000; Lanes 1–13 represent the F1 cloned pigs. NC, wild-type pigs; H_2O, blank control. "*" indicates a hybrid band formed in the process of genomic PCR in heterozygous animals. (C) Images of 3-month-old knockin and wild-type pigs. KI represents knockin; the intermuscular sulcus is indicated by a red arrow. (D) Levels of exogenous FSI-I-I and endogenous *MSTN* transcription in different tissues of knockin pigs. $*p < 0.05$, two-tailed unpaired t test. (E) Western blot analysis of *MSTN* expression in different skeletal muscle tissues. L, longissimus dorsi; G, gastrocnemius muscle; TP, trapezius pectoralis; TB, triceps brachii; B, biceps femoris; S, semitendinosus; (F) gray value analysis of *MSTN* expression in different skeletal muscle tissues using ImageJ. Values are denoted as the means ± SEM, n = 3, Student's t test. (G and I) The distribution of muscle fiber diameter in the longissimus dorsi and gastrocnemius from FSI-I-I knockin and wild-type pigs. At the age of 3 months, FSI-I-I knockin and wild-type pigs from the same litter were slaughtered, and their longissimus dorsalis and gastrocnemius muscles were removed for paraffin sectioning and statistical analysis of muscle fiber diameter. Values are denoted as the means ± SEM, n = 3, two-tailed unpaired t test, $*p < 0.05$, $**p < 0.01$, $***p < 0.001$. (H and J) Representative H&E-stained cross-sections of longissimus dorsi and gastrocnemius muscles from FSI-I-I knockin and wild-type pigs in the same litter.

of the high similarity of their anatomical and physiological characteristics to humans. Based on the results of the present study, we believe that *MSTN* inhibition via FSI-I-I overexpression in skeletal muscle could be used to treat muscle wasting diseases and diabetes.

In summary, in the present study, the HMEJ-based strategy mediated by CRISPR-Cas9 was shown to be a powerful approach for targeted gene integration in PFFs. To the best of our knowledge, this is the first study to generate FSI-I-I site-specific transgenic pigs using the HMEJ method, and the pigs exhibited a significant increase in muscle mass. The FSI-I-I gene mediates skeletal muscle hypertrophy, probably by acting on an *MSTN*-related signaling pathway and affecting the expression of myogenic regulatory factors. Moreover, FSI-I-I overexpression primarily affected skeletal muscles, with no adverse effects observed on other organs or tissues. Most importantly, due to the physiological similarity between humans and pigs, our FSI-I-I pigs can serve as therapeutic models for human muscular dystrophies and diabetes.

MATERIALS AND METHODS

Ethics statement

All animal studies were approved by the Animal Welfare and Research Ethics Committee at Jilin University, and all procedures were conducted in strict accordance with the Guide for the Care and Use of Laboratory Animals.

Vector construction

pRosa26-, pACTB-, and pMSTN-specific sgRNAs were cloned into pX330-U6-Chimeric_BB-CBh-hSpCas9 to produce functional Cas9/gRNA vectors, which were designated pX330-pRosa26, pX330-pACTB, and pX330-pMSTN, respectively. The sgRNA primers used in the present study are listed in Table S1. The EGFP fragment was amplified from plasmid pEGFP-N1, and the forward amplification primer contained the P2A sequence. The pRosa26 left HA (800 bp) and right HA (800 bp) sequences amplified from the wild-type pig genome and the EGFP fragment were used to construct the Rosa26-EGFP-Donor vector by overlap extension PCR. The HMEJ-Rosa26-EGFP-Donor sequence was sandwiched between 23-nt Rosa26-sgRNA sequences. The pACTB left HA (800 bp) and right HA (800 bp) sequences amplified from the wild-type pig genome and EGFP fragment were used to construct the ACTB-EGFP-Donor vector by overlap extension PCR. The HMEJ-ACTB-EGFP-Donor sequence was sandwiched between 23-nt ACTB-sgRNA sequences. The SA, P2A, and EGFP sequences are listed in Table S2. The HMEJ-FSI-I-I-Donor sequence was synthesized and purified through PAGE (GenScript, Nanjing, China).

Electroporation and selection of PFFs

PFFs isolated from 33-day-old large white fetuses were cultured in DMEM supplemented with 10% fetal bovine serum. Approximately 20 μg of Cas9/gRNA plasmids and 20 μg of donor plasmids were transfected into 3×10^6 cells using the Neon transfection system. The electroporation conditions used for PFFs were as follows: 1,350 V, 30 ms, 1 pulse. pX330-pMSTN- and HMEJ-FSI-I-I-Donor-cotransfected PFFs were seeded into 10-cm dishes at an appropriate density. When individual cell colonies formed, the cells were picked and transferred into 24-well plates. After recovery for 72 h, one-fifth of each cell colony was removed and lysed to provide a template for genotyping. The primer pairs 4F/R and 5F/R were used to detect site-specific knockin events. The nucleotide sequences of all primers used in the present study are presented in Table S1.

Flow cytometry analysis

Green fluorescent cells were analyzed by flow cytometry (BD FACSCelesta).

SCNT and genotype analysis

FSI-I-I knockin PFFs were used as donor cells for SCNT, which was performed based as described in previous studies.[75,76] Genomic DNA extracted from the newborn piglets was analyzed by PCR using the primer pairs 4F/R and 5F/R, and the PCR products were sequenced to confirm the knockin events.

Transcriptional analysis

Total RNA was extracted from the heart, liver, spleen, lungs, kidney, and longissimus dorsalis using an RNAsimple Total RNA Extraction Kit (Tiangen, Beijing, China). Approximately 1 μg of RNA was used to generate first-strand cDNA with FastKing gDNA Dispelling RT SuperMix (Tiangen, Beijing, China), and the resulting cDNA was used to perform real-time PCR. The primers used for real-time PCR are presented in Table S1.

T7E1 assay

T7E1 can recognize and cleave distorted dsDNA undergoing conformational changes.[77] PCR products covering 8 potential off-target sites were subjected to T7E1 digestion at 37°C for 30 min, and the reaction products were immediately subjected to agarose gel electrophoresis.

Western blotting analysis

Longissimus dorsalis samples of knockin and wild-type pigs were ground in liquid nitrogen, and NP40 lysis buffer was used to extract protein. Then, 30 μg of protein was separated by SDS-PAGE, and the protein bands were transferred to polyvinylidene difluoride membranes. Subsequently, the BSA-blotted membranes were separately incubated overnight with primary polyclonal antibodies against MSTN (Abcam, UK) diluted 1:250, FST (Abcam, UK) diluted 1:1,000, Smad2 (Novus, CO, USA) diluted 1:1,000, p-Smad2 (Novus, CO, USA) diluted 1:1,000, Smad3 (Novus, CO, USA) diluted 1:1,000, p-Smad3 (Novus, CO, USA) diluted 1:1,000, AKT (Cell Signaling Technology, MA, USA) diluted 1:1,000, p-AKT (Cell Signaling Technology, MA, USA) diluted 1:1,000, ERK (Cell Signaling Technology, MA, USA) diluted 1:1,000, and p-ERK (Cell Signaling Technology, MA, USA) diluted 1:1,000. Then, the membranes were washed 3 times with TBST and incubated for 1.5 h with horseradish peroxidase-coupled secondary antibodies diluted 1:5,000. The immunoblots were detected with ultrasensitive ECL chemiluminescence ready-to-use substrate (Boster, Wuhan, China).

Hematoxylin and eosin (H&E) staining

Longissimus dorsi and gastrocnemius samples obtained from 3-month-old knockin and wild-type pigs were fixed in 10% formalin for 24 h, and cross-sectioned muscle samples were then used to generate paraffin sections. Subsequently, images of the cross-sections stained with H&E were captured by microscopy (Olympus). Three representative areas from each muscle section were selected, and their myofiber areas were measured using ImageJ.

Off-target analysis

All potential off-target sites of *MSTN* locus were analyzed by T7E1 assays and Sanger sequencing. The PCR products spanning the potential off-target sites were digested with T7E1 and then analyzed by 2% agarose gel electrophoresis. Then, the digested PCR products were purified and sequenced.

Statistical analysis

Statistical analysis was performed by a two-tailed unpaired t test, and $p < 0.05$ was considered to indicate a significant difference.

SUPPLEMENTAL INFORMATION

Supplemental information can be found online at https://doi.org/10.1016/j.omtn.2021.06.011.

ACKNOWLEDGMENTS

This work was supported by Special Funds for Cultivation and Breeding of New Transgenic Organisms (number 2016ZX08006001), the Program for JLU Science and Technology Innovative Research Team (2017TD-28), and the Fundamental Research Funds for Central Universities.

AUTHOR CONTRIBUTIONS

M.L. performed the experiments and wrote the manuscript. X.T. wrote and revised the manuscript. D.P. and H.O. conceived the study. W.Y., Y.W., Y.C., and Y.L., contributed to data analysis. H.Y., C.G., X.C., and Z.X. performed portions of the experiments. All authors reviewed the manuscript.

DECLARATION OF INTERESTS

The authors declare no competing interests.

REFERENCES

1. Dankbar, B., Fennen, M., Brunert, D., Hayer, S., Frank, S., Wehmeyer, C., Beckmann, D., Paruzel, P., Bertrand, J., Redlich, K., et al. (2015). Myostatin is a direct regulator of osteoclast differentiation and its inhibition reduces inflammatory joint destruction in mice. Nat. Med. *21*, 1085–1090.
2. Amthor, H., Huang, R., McKinnell, I., Christ, B., Kambadur, R., Sharma, M., and Patel, K. (2002). The regulation and action of myostatin as a negative regulator of muscle development during avian embryogenesis. Dev. Biol. *251*, 241–257.
3. Shi, Y., and Massagué, J. (2003). Mechanisms of TGF-beta signaling from cell membrane to the nucleus. Cell *113*, 685–700.
4. McPherron, A.C., Lawler, A.M., and Lee, S.J. (1997). Regulation of skeletal muscle mass in mice by a new TGF-beta superfamily member. Nature *387*, 83–90.
5. Wang, K.K., Ouyang, H.S., Xie, Z.C., Yao, C.G., Guo, N.N., Li, M.J., Jiao, H.P., and Pang, D.X. (2015). Efficient Generation of Myostatin Mutations in Pigs Using the CRISPR/Cas9 System. Sci Rep *5*, 16623.
6. McPherron, A.C., and Lee, S.J. (1997). Double muscling in cattle due to mutations in the myostatin gene. Proc. Natl. Acad. Sci. USA *94*, 12457–12461.
7. Liu, W., Thomas, S.G., Asa, S.L., Gonzalez-Cadavid, N., Bhasin, S., and Ezzat, S. (2003). Myostatin is a skeletal muscle target of growth hormone anabolic action. J. Clin. Endocrinol. Metab. *88*, 5490–5496.
8. Iezzi, S., Di Padova, M., Serra, C., Caretti, G., Simone, C., Maklan, E., Minetti, G., Zhao, P., Hoffman, E.P., Puri, P.L., and Sartorelli, V. (2004). Deacetylase inhibitors increase muscle cell size by promoting myoblast recruitment and fusion through induction of follistatin. Dev. Cell *6*, 673–684.
9. Ueno, N., Ling, N., Ying, S.Y., Esch, F., Shimasaki, S., and Guillemin, R. (1987). Isolation and partial characterization of follistatin: a single-chain Mr 35,000 monomeric protein that inhibits the release of follicle-stimulating hormone. Proc. Natl. Acad. Sci. USA *84*, 8282–8286.
10. Matzuk, M.M., Lu, N., Vogel, H., Sellheyer, K., Roop, D.R., and Bradley, A. (1995). Multiple defects and perinatal death in mice deficient in follistatin. Nature *374*, 360–363.
11. Hashimoto, M., Shoda, A., Inoue, S., Yamada, R., Kondo, T., Sakurai, T., Ueno, N., and Muramatsu, M. (1992). Functional regulation of osteoblastic cells by the interaction of activin-A with follistatin. J. Biol. Chem. *267*, 4999–5004.
12. Phillips, D.J., and de Kretser, D.M. (1998). Follistatin: a multifunctional regulatory protein. Front. Neuroendocrinol. *19*, 287–322.
13. Zheng, H., Qiao, C., Tang, R., Li, J., Bulaklak, K., Huang, Z., Zhao, C., Dai, Y., Li, J., and Xiao, X. (2017). Follistatin N terminus differentially regulates muscle size and fat in vivo. Exp. Mol. Med. *49*, e377.
14. Schneyer, A.L., Sidis, Y., Gulati, A., Sun, J.L., Keutmann, H., and Krasney, P.A. (2008). Differential antagonism of activin, myostatin and growth and differentiation factor 11 by wild-type and mutant follistatin. Endocrinology *149*, 4589–4595.
15. Lee, S.J., Lee, Y.S., Zimmers, T.A., Soleimani, A., Matzuk, M.M., Tsuchida, K., Cohn, R.D., and Barton, E.R. (2010). Regulation of muscle mass by follistatin and activins. Mol. Endocrinol. *24*, 1998–2008.
16. Lee, S.J., and McPherron, A.C. (2001). Regulation of myostatin activity and muscle growth. Proc. Natl. Acad. Sci. USA *98*, 9306–9311.
17. Nakatani, M., Takehara, Y., Sugino, H., Matsumoto, M., Hashimoto, O., Hasegawa, Y., Murakami, T., Uezumi, A., Takeda, S., Noji, S., et al. (2008). Transgenic expression of a myostatin inhibitor derived from follistatin increases skeletal muscle mass and ameliorates dystrophic pathology in mdx mice. FASEB J. *22*, 477–487.
18. Leonetti, M.D., Sekine, S., Kamiyama, D., Weissman, J.S., and Huang, B. (2016). A scalable strategy for high-throughput GFP tagging of endogenous human proteins. Proc. Natl. Acad. Sci. USA *113*, E3501–E3508.
19. Stephens, C.J., Kashentseva, E., Everett, W., Kaliberova, L., and Curiel, D.T. (2018). Targeted in vivo knock-in of human alpha-1-antitrypsin cDNA using adenoviral delivery of CRISPR/Cas9. Gene Ther. *25*, 139–156.
20. Zhang, Y., Sastre, D., and Wang, F. (2018). CRISPR/Cas9 Genome Editing: A Promising Tool for Therapeutic Applications of Induced Pluripotent Stem Cells. Curr. Stem Cell Res. Ther. *13*, 243–251.
21. Yang, H., Wang, H., Shivalila, C.S., Cheng, A.W., Shi, L., and Jaenisch, R. (2013). One-step generation of mice carrying reporter and conditional alleles by CRISPR/Cas-mediated genome engineering. Cell *154*, 1370–1379.
22. Mali, P., Yang, L., Esvelt, K.M., Aach, J., Guell, M., DiCarlo, J.E., Norville, J.E., and Church, G.M. (2013). RNA-guided human genome engineering via Cas9. Science *339*, 823–826.
23. Cong, L., Ran, F.A., Cox, D., Lin, S., Barretto, R., Habib, N., Hsu, P.D., Wu, X., Jiang, W., Marraffini, L.A., and Zhang, F. (2013). Multiplex genome engineering using CRISPR/Cas systems. Science *339*, 819–823.
24. Cox, D.B.T., Platt, R.J., and Zhang, F. (2015). Therapeutic genome editing: prospects and challenges. Nat. Med. *21*, 121–131.
25. Srivastava, M., Nambiar, M., Sharma, S., Karki, S.S., Goldsmith, G., Hegde, M., Kumar, S., Pandey, M., Singh, R.K., Ray, P., et al. (2012). An inhibitor of nonhomologous end-joining abrogates double-strand break repair and impedes cancer progression. Cell *151*, 1474–1487.
26. Maruyama, T., Dougan, S.K., Truttmann, M.C., Bilate, A.M., Ingram, J.R., and Ploegh, H.L. (2015). Increasing the efficiency of precise genome editing with

CRISPR-Cas9 by inhibition of nonhomologous end joining. Nat. Biotechnol. *33*, 538–542.

27. Kurihara, T., Kouyama-Suzuki, E., Satoga, M., Li, X., Badawi, M., Thiha, Baig, D.N., Yanagawa, T., Uemura, T., Mori, T., and Tabuchi, K. (2020). DNA repair protein RAD51 enhances the CRISPR/Cas9-mediated knock-in efficiency in brain neurons. Biochem. Biophys. Res. Commun. *524*, 621–628.

28. Lin, S., Staahl, B.T., Alla, R.K., and Doudna, J.A. (2014). Enhanced homology-directed human genome engineering by controlled timing of CRISPR/Cas9 delivery. eLife *3*, e04766.

29. Charpentier, M., Khedher, A.H.Y., Menoret, S., Brion, A., Lamribet, K., Dardillac, E., Boix, C., Perrouault, L., Tesson, L., Geny, S., et al. (2018). CtIP fusion to Cas9 enhances transgene integration by homology-dependent repair. Nat. Commun. *9*, 1133.

30. Ma, M., Zhuang, F., Hu, X., Wang, B., Wen, X.Z., Ji, J.F., and Xi, J.J. (2017). Efficient generation of mice carrying homozygous double-floxp alleles using the Cas9-Avidin/Biotin-donor DNA system. Cell Res. *27*, 578–581.

31. Yao, X., Wang, X., Hu, X., Liu, Z., Liu, J., Zhou, H., Shen, X., Wei, Y., Huang, Z., Ying, W., et al. (2017). Homology-mediated end joining-based targeted integration using CRISPR/Cas9. Cell Res. *27*, 801–814.

32. Wierson, W.A., Welker, J.M., Almeida, M.P., Mann, C.M., Webster, D.A., Torrie, M.E., Weiss, T.J., Kambakam, S., Vollbrecht, M.K., Lan, M., et al. (2020). Efficient targeted integration directed by short homology in zebrafish and mammalian cells. eLife *9*, e53968.

33. Saito, T., Matsuba, Y., Mihira, N., Takano, J., Nilsson, P., Itohara, S., Iwata, N., and Saido, T.C. (2014). Single App knock-in mouse models of Alzheimer's disease. Nat. Neurosci. *17*, 661–663.

34. Miura, H., Quadros, R.M., Gurumurthy, C.B., and Ohtsuka, M. (2018). Easi-CRISPR for creating knock-in and conditional knockout mouse models using long ssDNA donors. Nat. Protoc. *13*, 195–215.

35. Song, Y., Zhang, Y., Chen, M., Deng, J., Sui, T., Lai, L., and Li, Z. (2018). Functional validation of the albinism-associated tyrosinase T373K SNP by CRISPR/Cas9-mediated homology-directed repair (HDR) in rabbits. EBioMedicine *36*, 517–525.

36. Yang, D.S., Song, J., Zhang, J.F., Xu, J., Zhu, T.Q., Wang, Z., Lai, L.X., and Chen, Y.E. (2016). Identification and characterization of rabbit ROSA26 for gene knock-in and stable reporter gene expression. Sci Rep *6*, 25161.

37. Wang, K.K., Tang, X.C., Liu, Y., Xie, Z.C., Zou, X.D., Li, M.J., Yuan, H.M., Ouyang, H.S., Jiao, H.P., and Pang, D.X. (2016). Efficient Generation of Orthologous Point Mutations in Pigs via CRISPR-assisted ssODN-mediated Homology-directed Repair. Mol Ther Nucleic Acids *5*, e396.

38. Zou, X., Ouyang, H., Yu, T., Chen, X., Pang, D., Tang, X., and Chen, C. (2019). Preparation of a new type 2 diabetic miniature pig model via the CRISPR/Cas9 system. Cell Death Dis. *10*, 823.

39. Niu, D., Wei, H.J., Lin, L., George, H., Wang, T., Lee, I.H., Zhao, H.Y., Wang, Y., Kan, Y., Shrock, E., et al. (2018). Inactivation of porcine endogenous retrovirus in pigs using CRISPR-Cas9. Transgenic Res. *27*, 483–483.

40. Yan, S., Tu, Z., Liu, Z., Fan, N., Yang, H., Yang, S., Yang, W., Zhao, Y., Ouyang, Z., Lai, C., et al. (2018). A Huntingtin Knockin Pig Model Recapitulates Features of Selective Neurodegeneration in Huntington's Disease. Cell *173*, 989–1002.e13.

41. Li, M.J., Ouyang, H.S., Yuan, H.M., Li, J.N., Xie, Z.C., Wang, K.K., Yu, T.T., Liu, M.H., Chen, X., Tang, X.C., et al. (2018). Site-Specific Fat-1 Knock-In Enables Significant Decrease of n-6PUFAs/n-3PUFAs Ratio in Pigs. G3-Genes Genom Genet *8*, 1747–1754.

42. Langley, B., Thomas, M., Bishop, A., Sharma, M., Gilmour, S., and Kambadur, R. (2002). Myostatin inhibits myoblast differentiation by down-regulating MyoD expression. J. Biol. Chem. *277*, 49831–49840.

43. Yang, W., Chen, Y., Zhang, Y., Wang, X., Yang, N., and Zhu, D. (2006). Extracellular signal-regulated kinase 1/2 mitogen-activated protein kinase pathway is involved in myostatin-regulated differentiation repression. Cancer Res. *66*, 1320–1326.

44. Trendelenburg, A.U., Meyer, A., Rohner, D., Boyle, J., Hatakeyama, S., and Glass, D.J. (2009). Myostatin reduces Akt/TORC1/p70S6K signaling, inhibiting myoblast differentiation and myotube size. Am. J. Physiol. Cell Physiol. *296*, C1258–C1270.

45. Zammit, P.S. (2017). Function of the myogenic regulatory factors Myf5, MyoD, Myogenin and MRF4 in skeletal muscle, satellite cells and regenerative myogenesis. Semin. Cell Dev. Biol. *72*, 19–32.

46. Xie, Z., Pang, D., Yuan, H., Jiao, H., Lu, C., Wang, K., Yang, Q., Li, M., Chen, X., Yu, T., et al. (2018). Genetically modified pigs are protected from classical swine fever virus. PLoS Pathog. *14*, e1007193.

47. Chu, V.T., Weber, T., Wefers, B., Wurst, W., Sander, S., Rajewsky, K., and Kühn, R. (2015). Increasing the efficiency of homology-directed repair for CRISPR-Cas9-induced precise gene editing in mammalian cells. Nat. Biotechnol. *33*, 543–548.

48. Robert, F., Barbeau, M., Éthier, S., Dostie, J., and Pelletier, J. (2015). Pharmacological inhibition of DNA-PK stimulates Cas9-mediated genome editing. Genome Med. *7*, 93.

49. Xie, Z.C., Pang, D.X., Wang, K.K., Li, M.J., Guo, N.N., Yuan, H.M., Li, J.N., Zou, X.D., Jiao, H.P., Ouyang, H.S., et al. (2017). Optimization of a CRISPR/Cas9-mediated Knock-in Strategy at the Porcine Rosa26 Locus in Porcine Foetal Fibroblasts. Sci Rep *7*, 3036.

50. McCreath, K.J., Howcroft, J., Campbell, K.H.S., Colman, A., Schnieke, A.E., and King, A.J. (2000). Production of gene-targeted sheep by nuclear transfer from cultured somatic cells (vol 405, pg 1066, 2000). Nature *408*, 120.

51. Lee, G.S., Hyun, S.H., Kim, H.S., Kim, D.Y., Lee, S.H., Lim, J.M., Lee, E.S., Kang, S.K., Lee, B.C., and Hwang, W.S. (2003). Improvement of a porcine somatic cell nuclear transfer technique by optimizing donor cell and recipient oocyte preparations. Theriogenology *59*, 1949–1957.

52. Lee, S.J. (2004). Regulation of muscle mass by myostatin. Annu. Rev. Cell Dev. Biol. *20*, 61–86.

53. Tsuchida, K. (2008). Myostatin inhibition by a follistatin-derived peptide ameliorates the pathophysiology of muscular dystrophy model mice. Acta Myol. *27*, 14–18.

54. Han, X.Q., Moller, L.L.V., De Groote, E., Bojsen-Moller, K.N., Davey, J., Henriquez-Olguin, C., Li, Z.C., Knudsen, J.R., Jensen, T.E., Madsbad, S., et al. (2019). Mechanisms involved in follistatin-induced hypertrophy and increased insulin action in skeletal muscle. J Cachexia Sarcopeni *10*, 1241–1257.

55. Chang, F., Fang, R., Wang, M., Zhao, X., Chang, W., Zhang, Z., Li, N., and Meng, Q. (2017). The transgenic expression of human follistatin-344 increases skeletal muscle mass in pigs. Transgenic Res. *26*, 25–36.

56. Norris, A.L., Lee, S.S., Greenlees, K.J., Tadesse, D.A., Miller, M.F., and Lombardi, H.A. (2020). Template plasmid integration in germline genome-edited cattle. Nat. Biotechnol. *38*, 163–164.

57. Xie, L., Sun, J., Mo, L., Xu, T., Shahzad, Q., Chen, D., Yang, W., Liao, Y., and Lu, Y. (2019). HMEJ-mediated efficient site-specific gene integration in chicken cells. J. Biol. Eng. *13*, 90.

58. Muttukrishna, S., Tannetta, D., Groome, N., and Sargent, I. (2004). Activin and follistatin in female reproduction. Mol. Cell. Endocrinol. *225*, 45–56.

59. Chen, W.J.Y., Greulich, S., van der Meer, R.W., Rijzewijk, L.J., Lamb, H.J., de Roos, A., Smit, J.W.A., Romijn, J.A., Ruige, J.B., Lammertsma, A.A., et al. (2013). Activin A is associated with impaired myocardial glucose metabolism and left ventricular remodeling in patients with uncomplicated type 2 diabetes. Cardiovasc. Diabetol. *12*, 150.

60. Chen, W.J.Y., Greulich, S., Rijzewijk, L.J., van der Meer, R.W., Bekaert, M., Lamb, H.J., de Roos, A., Romijn, J.A., Smit, J.W.A., Vandenplas, G., et al. (2012). Activin A is derived from human epicardial adipose tissue and associates with decreased myocardial function and glucose metabolism in human diabetic cardiomyopathy. Diabetologia *55*, S495–S495.

61. Hashimoto, O., and Funaba, M. (2011). Activin in glucose metabolism. Vitam. Horm. *85*, 217–234.

62. Hashimoto, O., Sekiyama, K., Matsuo, T., and Hasegawa, Y. (2009). Implication of activin E in glucose metabolism: transcriptional regulation of the inhibin/activin betaE subunit gene in the liver. Life Sci. *85*, 534–540.

63. Hashimoto, M., Nakamura, T., Inoue, S., Kondo, T., Yamada, R., Eto, Y., Sugino, H., and Muramatsu, M. (1992). Follistatin is a developmentally regulated cytokine in neural differentiation. J. Biol. Chem. *267*, 7203–7206.

64. Mayer, K., Buchbinder, A., and Morty, R.E. (2012). Activin A: a mediator governing inflammation, immunity, and repair. Am. J. Respir. Crit. Care Med. *185*, 350–352.

65. Qi, L.S., Larson, M.H., Gilbert, L.A., Doudna, J.A., Weissman, J.S., Arkin, A.P., and Lim, W.A. (2013). Repurposing CRISPR as an RNA-guided platform for sequence-specific control of gene expression. Cell *152*, 1173–1183.

66. Bellinge, R.H.S., Liberles, D.A., Iaschi, S.P.A., O'brien, P.A., and Tay, G.K. (2005). Myostatin and its implications on animal breeding: a review. Anim. Genet. *36*, 1–6.

67. Cash, J.N., Rejon, C.A., McPherron, A.C., Bernard, D.J., and Thompson, T.B. (2009). The structure of myostatin:follistatin 288: insights into receptor utilization and heparin binding. EMBO J. *28*, 2662–2676.

68. Rudnicki, M.A., Schnegelsberg, P.N., Stead, R.H., Braun, T., Arnold, H.H., and Jaenisch, R. (1993). MyoD or Myf-5 is required for the formation of skeletal muscle. Cell *75*, 1351–1359.

69. Knapp, J.R., Davie, J.K., Myer, A., Meadows, E., Olson, E.N., and Klein, W.H. (2006). Loss of myogenin in postnatal life leads to normal skeletal muscle but reduced body size. Development *133*, 601–610.

70. Moretti, I., Ciciliot, S., Dyar, K.A., Abraham, R., Murgia, M., Agatea, L., Akimoto, T., Bicciato, S., Forcato, M., Pierre, P., et al. (2016). MRF4 negatively regulates adult skeletal muscle growth by repressing MEF2 activity. Nat. Commun. *7*, 12397.

71. Moyer, A.L., and Wagner, K.R. (2011). Regeneration versus fibrosis in skeletal muscle. Curr. Opin. Rheumatol. *23*, 568–573.

72. Akpan, I., Goncalves, M.D., Dhir, R., Yin, X., Pistilli, E.E., Bogdanovich, S., Khurana, T.S., Ucran, J., Lachey, J., and Ahima, R.S. (2009). The effects of a soluble activin type IIB receptor on obesity and insulin sensitivity. Int. J. Obes. *33*, 1265–1273.

73. Guo, T., Jou, W., Chanturiya, T., Portas, J., Gavrilova, O., and McPherron, A.C. (2009). Myostatin inhibition in muscle, but not adipose tissue, decreases fat mass and improves insulin sensitivity. PLoS ONE *4*, e4937.

74. Tang, R., Harasymowicz, N.S., Wu, C.L., Collins, K.H., Choi, Y.R., Oswald, S.J., and Guilak, F. (2020). Gene therapy for follistatin mitigates systemic metabolic inflammation and post-traumatic arthritis in high-fat diet-induced obesity. Sci. Adv. *6*, eaaz7492.

75. Lai, L., Kolber-Simonds, D., Park, K.W., Cheong, H.T., Greenstein, J.L., Im, G.S., Samuel, M., Bonk, A., Rieke, A., Day, B.N., et al. (2002). Production of alpha-1,3-galactosyltransferase knockout pigs by nuclear transfer cloning. Science *295*, 1089–1092.

76. Lai, L., Kang, J.X., Li, R., Wang, J., Witt, W.T., Yong, H.Y., Hao, Y., Wax, D.M., Murphy, C.N., Rieke, A., et al. (2006). Generation of cloned transgenic pigs rich in omega-3 fatty acids. Nat. Biotechnol. *24*, 435–436.

77. Déclais, A.C., and Lilley, D.M.J. (2008). New insight into the recognition of branched DNA structure by junction-resolving enzymes. Curr. Opin. Struct. Biol. *18*, 86–95.